I.A.U
Karaj branch

Journal of
A p p l ied
C hemical
R esearch
jacr.kiau.ac.ir

Journal of Applied Chemical Research, 18, 1, 88-107 (2024)

Removal of Benzyl Paraben from Wastewater Using Zeolitic Imidazolate-67 Modified by Fe_3O_4 Nanoparticles with Response Surface Methodology

Mohammad Pourmohammad[1], Arezoo Ghadi[1]*, Ali Aghababai Beni[2]

[1]*Department of Chemical Engineering, Ayatollah Amoli Branch, Islamic Azad University, Amol, Iran*

[2]*Department of Chemical Engineering, Shahrekord Branch, Islamic Azad University, Shahrekord, Iran*

(Received 18 May 2023; Final revised received 22 Aug. 2023)

Abstract

The applicability of Zeolitic Imidazolate-67, Modified by Fe_3O_4 Nanoparticles, was studied for the removal of benzyl paraben from wastewater by adsorption method studied using response surface methodology (RSM). For the adsorption characterization of the adsorbent used in benzyl paraben adsorption, BET, FTIR, XRD, and SEM analyses were performed. The impacts of variables including initial benzyl paraben concentration (X_1), pH (X_2), adsorbent dosage (X_3), and sonication time (X_4) came under scrutiny using response surface methodology (RSM). The values of 10 mg L^{-1}, 0.03 g, 7.0, and 4.0 min were considered as the ideal values for benzyl paraben concentration, adsorbent, pH, and contact time, respectively. Adsorption equilibrium and kinetic data were fitted with the Langmuir monolayer isotherm model and pseudo-second-order kinetics (R^2: 0.999) with maximum adsorption capacity (92.0 mgg^{-1}), respectively. The predicted values were in agreement with experimental values obtained for the components of the mixture. The values at the optimized process conditions indicated a commercially viable route for optimal removal of dyes from wastewater.

Keywords: Benzyl Paraben, Zeolitic Imidazolate-67, Central Composite Design (CCD), Response Surface Methodology (RSM), Wastewater.

***Corresponding author:** Arezoo Ghadi, Department of Chemical Engineering, Ayatollah Amoli Branch, Islamic Azad University, Amol, Iran, E-mail: arezoo.ghadi@gmail.com*

Introduction

Industrial wastewater as an undesirable by-product may be released to a sanitary sewer or surface water in the environment. Therefore, this issue has been among the most serious environmental concerns to keep an eye on. It requires considerable time and effort to blanch their high color and organic concentrations [1]. Parabens are chemical esters of p-hydroxybenzoic acid and are a class of widely used artificial preservatives and antimicrobial in many PCPs (personal care products) as well as pharmaceutical products [2], food, beverages, and industrial products. The use of parabens in sunscreen creams, toothpastes, cosmetics, glues, fats, and oils is inevitable and their use in a variety of consumer products is undeniable [3]. Also, some scholars in their published studies have associated the high concentrations of parabens with male reproductive disorders. However, paraben has found its way to wastewater plants due to its large mentioned application. Some wastewater treatment technologies were successful in removing a considerable amount of paraben from wastewater [4]. Moreover, the presence of parabens in soil and sediment samples has been confirmed. Accordingly, the necessity of removing toxic dyes from industrial wastewater has turned into a global concern [5]. For removing dyes from aqueous media, different methods of coagulation, precipitation, adsorption, membrane filtration, electrochemical techniques, ozonation, and bio sorption have been practiced [6-9]. Particularly, adsorption has drawn the attention of worldwide researcher's, thanks to its simplicity in operation, high efficiency, and its inexpensive operation cost [10,11]. In improving removal efficiency, detecting novel adsorbent materials has always been the most prominent issue in adsorption [12].

Conventional adsorbents, in terms of selectivity and capacity, have emerged as a fundamental problem. In recent years, metal-organic frameworks (MOFs), owing to their high surface area and porosity, high adsorption capacity, and desirable guest-host interactions, have been employed as a promising alternative in various applications such as drug delivery, and adsorption processes [13,14]. Zeolitic Imidazolate Frameworks (ZIFs) represent a particular class of Metal-Organic Frameworks (MOFs), formed by imidazole linkers and zinc or cobalt ions, resulting in microporous crystalline structures with characteristics of both MOFs and zeolites [15,16]. ZIFs possess unique porous structures with open frameworks, adjustable cage pore structures, large surface areas, great functionalities, and enhanced thermal and chemical stabilities, which led them to a wide range of potential applications, including adsorption, catalysis, separation, and sensing [17-20].

The high adsorption capacity of the MOFs has to the electrostatic interactions, conjugated π-π interactions, and hydrogen bonds. Since the MOFs show good thermal and chemical stability, various applications, include gas adsorption, molecular separation, and electrochemistry. One of the most studied metal-organic frameworks is the Zeolite Imidazolate-67 (ZIF-67), which consists of

Co^{2+} ions linked by 2-methyl imidazolate to create a crystalline cubic structure with the parameters a = b = c = 16.9585 Å. ZIF-67 offers a three-dimensional (3D) structure with a high tendency to adsorb contaminants in the aqueous media. However, the application of ZIF-67 as an adsorbent still faces three vital problems, including low specific surface area, poor structural stability, and difficult separation [21,22]. Iron oxide nanoparticles are widely used for metal remediation due to their low toxicity and easy separation from water media in addition, where the nanoparticle (NP) is composed of magnetite, a facile magnetic separation of NPs, along with associated contaminants, can be performed. However, bare magnetite nanoparticles rapidly aggregate in aqueous systems and are highly susceptible to transformations under many environmental conditions [23,24].

Nowadays, the fashion business has a significant development, which may contribute to textile dye development faster. Thereby, dye chemicals have higher color stability under light. However, wastewater from the dye industry will be more to handle. Among modern treatment technologies, adsorption is an effective treatment [25,26]. Zeolitic Imidazolates are modified by containing iron ions (Fe^{2+} or Fe^{3+}), which are involved in complex mechanisms of reactions such as photo, electro, ultrasonic, or combination processes [27,28]. The relatively high saturation magnetization values of ZIF-67-Fe_3O_4NPs make it susceptible to magnetic fields and easy to separate from aqueous solutions. The absence of significant hysteresis, remanence, ZIF-67-Fe_3O_4NPs, which is crucial for adsorption and removal materials [29,30].

The synthesis of these unique adsorbents named ZIF-67 Modified by Fe_3O_4NPs was easily carried out and subsequently through the instrumentality of scanning electron microscopy (SEM), Fourier transform infrared spectroscopy (FTIR) and X-ray diffraction (XRD) analysis, they were characterized. Therefore, preparing ZIF-67 Modified by Fe_3O_4NPs as an alternative to exorbitant or noxious adsorbents for the elimination of (BP) dye from wastewater attracted our attention. In the process of (BP) dye deletion, shown structured benzyl paraben (BP) dye in Fig. 1, In (BP) dye elimination process, with the help of CCD (central composite design) under RSM (response surface methodology). This fact that the adsorption of benzyl paraben follows the pseudo-second-order rate equation was clearly proven. Furthermore, it was demonstrated that the Langmuir model could undoubtedly be used for the equilibrium data explanation. The pseudo-second-order model was in control of the kinetic of adsorption process which was confirmed through the analysis of kinetic models (both pseudo-first-order, pseudo-second-order diffusion models). The capability of ZIF-67 Modified by Fe_3O_4NPs in eliminating of (BP) dye from wastewater was demonstrated by evidences.

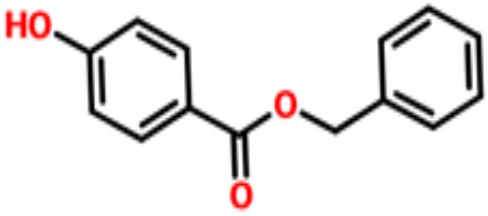

Figure 1. The structures of Benzyl Paraben (BP).

Experimental

Chemical and instruments

All the chemicals used are of the highest purity, and purchased from Merck (Darmstadt, Germany). Benzyl paraben (BP) dye (97%), Ammonium heptamolybdate (99%), and Iron nitrate (III) (98.0%). The standard and experimental solutions were obtained by diluting the stock solutions with deionized water. The applied instruments were as follow: Dyes concentrations were determined using Jasco UV–Vis spectrophotometer model V-530 (Jasco Company, Japan). IR spectra were registered on a (PerkinElmer company, Germany). SEM (Phillips, PW3710, Netherland), used to study the morphology of samples.

Synthesis of ZIF-67 Modified by Fe_3O_4NPs

Synthesis ZIF-67 Modified by Fe_3O_4NPs were as follows: first, 0.86 g of $FeCl_2{\cdot}4H_2O$, 2.35 g $FeCl_3{\cdot}6H_2O$ (molar ratio of Fe^{2+}: Fe^{3+}=1:2), and 40 ml of NH_4OH (25%) solution is mixed and placed under N_2 gas for 2 h at 90 °C under stirrer condition [24]. We used an ultrasonic bath, in the solution containing, 0.36 g of $Co(NO_3)_2.6H_2O$, 0.75 g of 2-methylimidazole, and 0.405 g of HCOO-Na in 60 mL of methanol for ZIF-67. The mixture was refluxed at 60°C for 24 h under N_2 gas. After cooling to room temperature, the mixture was centrifuged (3000 rpm, 15 min, 15°C). The solids were left to soak for 24 h methanol, and centrifuged until be separated the colorless supernatant was, and dried at 80 °C. The sorbent ZIF-67 Modified by Fe_3O_4NPs with an equal weight ratio, the stirring, and the sediment suspension in the laboratory for 2 hours produced [22,30].

Adsorption experiments

Based on the experimental conditions in the CCD, the adjustment of the pH of different solutions with different concentration of (BP) dye was carried out utilizing concentrated HCl and/or NaOH. Through using an Erlenmeyer flask (50 mL), they were mixed completely with exact amounts of absorbent. The trials were done at ambient temperature during predetermined sonication time in an ultrasonic. In the twilight of the adsorption process, the centrifugation of the sample solution was

done promptly and the analysis of the supernatant containing residual was performed using UV-Vis spectroscopy. The computation of the removal percentage of (BP) dye (R %) during a given period and the calculation of the amount of (BP) dye adsorbed after reaching the equilibrium (qe (mg g^{-1})) was done using the ensuing equations:

$$R\% = \frac{C_{oi} - C_{ei}}{C_{0i}} \times 100 \quad (1)$$

$$q_i = \frac{V(C_{oi} - C_{ei})}{W} \times 100 \quad (2)$$

C_0 (mg/L) in the above equation pertains to the initial (BP) dye concentration, and C_e (mg/L) also signifies the equilibrium dyes concentration in aqueous solution. The solution volume is shown by V (L), and the adsorbent mass is demonstrated by W (g) [31,32].

Ultrasound Assisted method

Through the instrumentality of ultrasound assisted method, the elimination of (BP) dye in an adsorption combined with ZIF-67 Modified by Fe_3O_4 NPs was scrutinized. In a batch mode, the sonochemical adsorption trial was performed in the following way: the Erlenmeyer flask was loaded with exact quantities of (BP) dye solution (50 mL) at specified concentration 10.0 mg L^{-1}, and pH of 7.0 with a known quantity of adsorbent (0.03 g) while the desired sonication time (4 min) was maintained at the 25°C. It is worth mentioning that all utilized solutions were prepared per day with desired concentrations by diluting the stock solution with DW (double distilled water). The adsorption trials were executed in a batch mode and the solution was ultrasonicated at conditions devised under RSM. After performing the centrifugation for 4 min, the adsorbent ZIF-67 Modified by Fe_3O_4 NPs were separated. The analysis of the dilute phase was done for determining (BP) dye concentration with the help of UV–Vis spectrophotometer at wavelength of 370 nm [6, 32].

Central composite design (CCD)

The central composite design, for modeling, and the optimization of the effects of concentration of (BP) dye (X_1), pH (X_2), amount of adsorbent (X_3), and contact time (X_4) on the ultrasonic-assisted adsorption of (BP) dye by ZIF-67 Modified by Fe_3O_4 NPs. Four levels at which the R% of (BP) dye as a response was determined and shown in (Tables 1 and 2). To evaluate the essential, and effective terms for modeling the answer based on *F*-test. *P*-values less than 0.05 are generally considered a criterion for distinguishing statistically significant variables [32,33].

Table 1. Experimental factors, levels, and matrix of CCD.

Factors	levels			Star pointα = 2.0	
	Low (-1)	Central (0)	High(+1)	-α	+α
(X_1) (BP) dye Concentration (mg L^{-1})	10	15	20	5	25
(X_2) pH	4.0	6.0	8.0	2.0	10.0
(X_3) Adsorbent mass (g)	0.0125	0.025	0.03	0.0075	0.035
(X_4) Sonication time (min)	3.0	4.0	6.0	2.0	8.0

Desirability function

Desirability function or DF designs a function for each specific response that provokes the final output of the general function (D) and the highest value of this output guarantees the achievement of optimum value. The governing principle and application of desirability function for the finest prognostication of real behavior of sorption system was mentioned before [32,33]. In the desirability profiles, the predicted levels of variables that can create the most favorable responses are recorded.

Table 2. The design and the response.

Run	X_1	X_2	X_3	X_4	R% (BP) dye
1	20	6	0.025	4	93.0
2	30	8	0.0125	3	65.0
3	10	4	0.0125	6	96.0
4	20	6	0.025	4	94.0
5	30	4	0.0125	3	74.0
6	10	8	0.03	3	99.2
7	20	4	0.025	4	97.0
8	20	6	0.025	8	95.0
9	30	4	0.03	3	83.0
10	30	4	0.0125	5	91.0
11	20	6	0.025	4	94.6
12	30	8	0.0125	6	72.0
13	30	8	0.03	6	81.0
14	10	8	0.0125	3	96.0
15	20	6	0.025	4	93.0
16	30	4	0.03	6	94.2
17	20	6	0.025	4	94.1

18	10	4	0.0125	3	94.4
19	10	8	0.0125	6	98.2
20	10	4	0.03	6	96.0
21	10	8	0.03	6	100.0
22	40	6	0.0125	4	60.2
23	30	8	0.03	3	66.0
24	20	6	0.025	4	94.3
25	20	6	0.025	4	94.6
26	20	6	0.0075	4	91.2
27	20	6	0.025	2	46.0
28	20	10	0.025	4	84.0
29	10	4	0.03	3	96.0
30	20	6	0.035	4	99.2

Results and discussion

Characterization of absorbent

BET analysis of ZIF-67 Modified by Fe_3O_4 NPs.

BET analysis was used to study the physicochemical properties of ZIF-67 Modified by Fe_3O_4 NPs. Figure 2a shows the related N_2 adsorption-desorption isotherm, which clearly exhibits a type-IV isotherm with a noticeable hysteresis loop in the P/P_0 region of 0.3-0.95. The corresponding N_2 adsorption-desorption isotherm is shown in Figure 2a, where a type-IV isotherm is clearly visible with a distinct hysteresis loop in the P/P_0 range of 0.3-0.95. The specific surface area of the ZIF-67 Modified by Fe_3O_4 NPs was found to be 203.78 $m^2.g^{-1}$. The corresponding BJH pore distribution curve (Figure 2b) was used to evaluate the pore structure of ZIF-67 Modified by Fe_3O_4 NPs. As can be seen, two distinct types of pores were observed: microspores (2 nm) and mesospores (2-50 nm), with an average pore width of 4.179 nm [22,34].

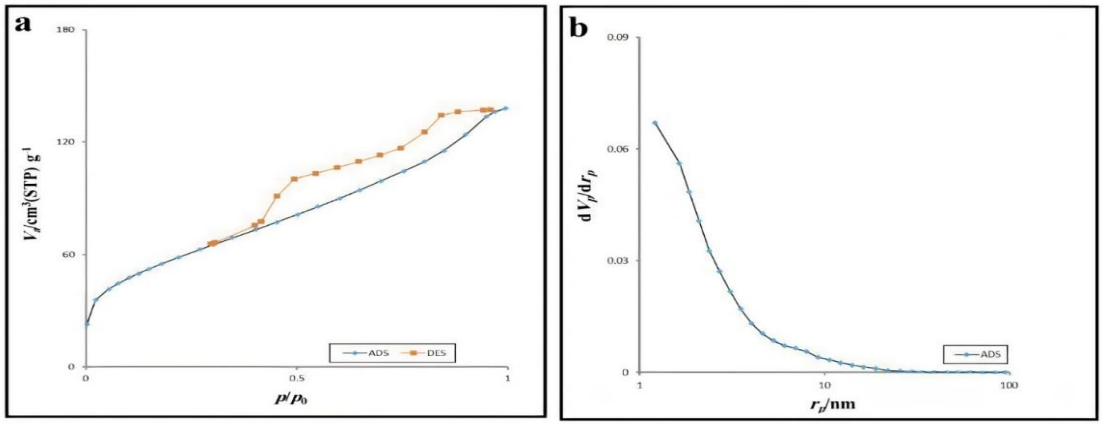

Figure 2. (a) The N2 adsorption-desorption isotherm of ZIF-67 Modified by Fe_3O_4 NPs, and (b) its corresponding BJH pore distribution curve.

FT-IR, XRD, and SEM analysis

FT-IR, XRD, and SEM measurements to characterize the adsorbent structural characterization. Figure 3a, all FT-IR spectra exhibit broadband covering the 3300 to 3500 cm^{-1} range, with an absorption band observed at 3378 cm^{-1} for stretching vibrations of OH groups and C-H bonds, respectively. The characteristic band at 1590 cm^{-1} is consistent with the C=N stretching vibrations in ZIF67. The FT-IR spectra of ZIF-67-Fe_3O_4NPs showed distinct peaks of ZIF-67, indicating vibrations. The rise, at 1055 and 1392 cm^{-1} confirmed the presence of benzene rings. The peak was also, at 572 cm^{-1} for Fe-O-Fe bonds in the Fe_3O_4 nanoparticles [22,34]. Figure 3b, shows the X-ray diffraction (XRD) patterns of Fe_3O_4NPs, ZIF-67, and ZIF-67-Fe_3O_4NPs. The presence of characteristic peaks of ZIF-67 and Fe_3O_4NPs in the XRD patterns- of ZIF-67-Fe_3O_4NPs confirms the formation of Fe_3O_4NPs in the XRD patterns of ZIF-67-Fe_3O_4NPs. The characteristic peaks of ZIF-67-Fe_3O_4NPs at 2θ = 63.06º, 57.23º, 53.73º, 43.34º, 35.75º, and 30.38º, respectively, corresponding to (440), (511), (422), (400), (311), and (220) planes, correspond to the characteristic peaks of Fe_3O_4NPs, indicating that the crystal structure of ZIF-67-Fe_3O_4NPs is intact and there was no serious crystallographic disruption in ZIF-67 by the incorporation of Fe_3O_4NPs, during the synthesis [34,35]. A morphological study of the ZIF-67-Fe_3O_4NPs was carried out by SEM. The surface morphology of the ZIF-67-Fe_3O_4NPs is in (Figure 4). Clearly, the ZIF-67-Fe_3O_4NPs are formed of many ultrafine nanoparticles in the range of 36-55 nm [35].

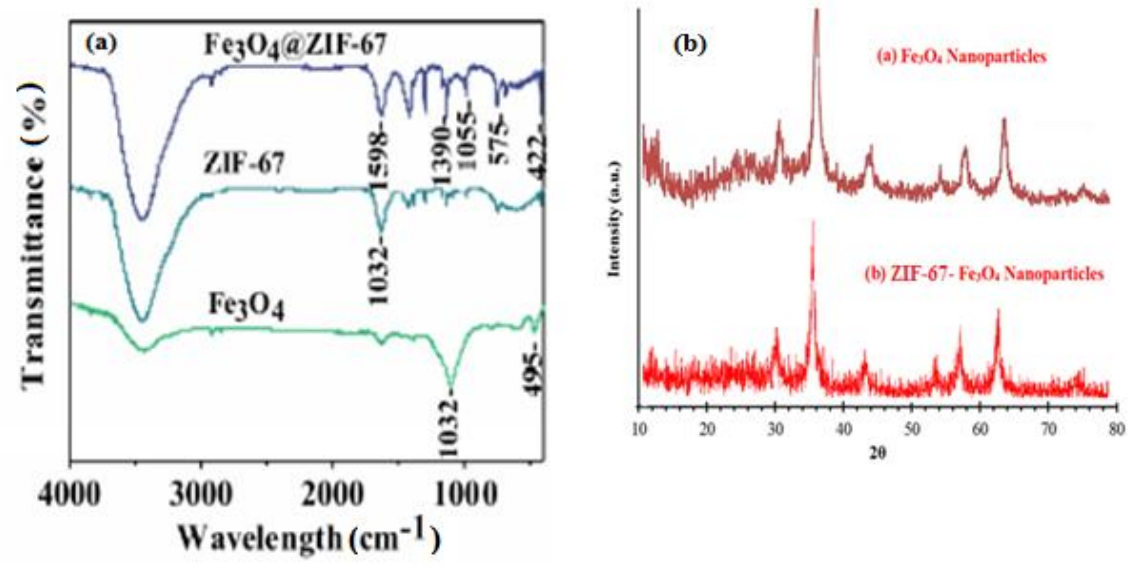

Figure. 3. (a) FTIR spectra of the prepared Fe_3O_4NPs, ZIF-67, ZIF-67-Fe_3O_4NPs. (b) Comparison of the XRD pattern of Fe_3O_4 NPs, and ZIF-67-Fe_3O_4NPs.

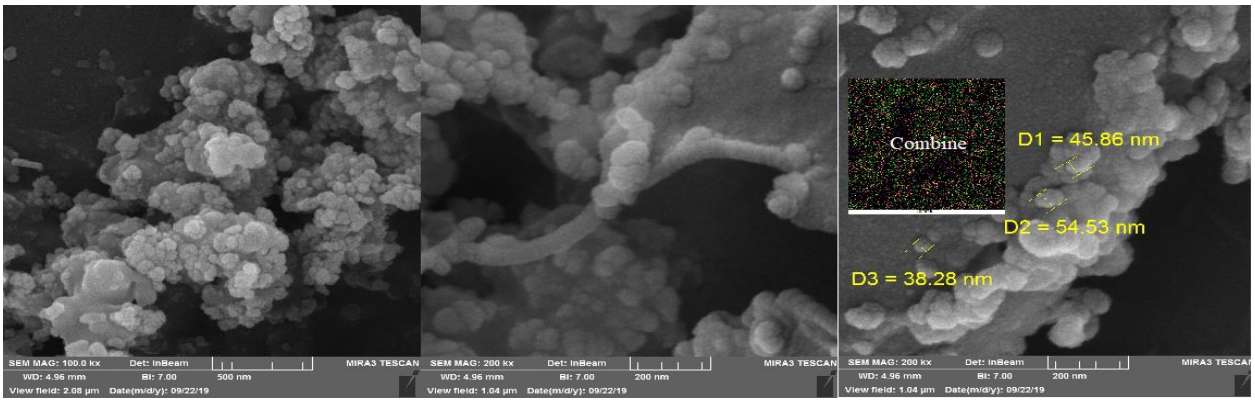

Figure 4. The (SEM) image of the ZIF-67-Fe_3O_4NPs.

Modeling the process and statistical analysis

The variance analysis of all the linear, quadratic and interaction impacts of the three planning factors in relation to R% of (BP) dye is represented in (Table 3). As specified by the F-value and p-value (<0.05), the model was extremely successful in elimination of dyes in the polynomial equation with 95% confidence interval [31,36]. By considering the value of the determination coefficient for deleting dye, it has been noticed that the response surface quadratic model was a befitting model for predicting the function of dye adsorption on ZIF-67-Fe_3O_4NPs. The plots of experimental deletion % when juxtaposed against those computed from equations revealed a satisfactory fit (Eq. 3). Represents the codified values for the quadratic equations after ruling out the insignificant terms.

$$R\%\ (BP)dye = 93/084 - 10/093X_1 - 3/340X_2 + +2/4167X_3 + 4/2700X_4 - 4/9075X_1X_2 - 1/3925X_1X_3 + 3/5525X_1X_4 + 0/89500X_2X_3 - 0/17500X_2X_4 - 0/44000X_3X_4 - 3/7119X_1^2 - 1/1059X_2^2 + 0/39410X_3^2 - 2/3559X_4^2 \quad (3)$$

where Y shows the predicted response (R% of dye), and the coded value of X_1 stands for the initial (BP) dye concentrations, X_2 for pH, X_3 and X_4 for the adsorbent mass and ultrasound time respectively. The significance of X1, X_2, X_4, X_5, X_1X_3, X_1X_4 and all quadratic impacts for R% of (BP) dye was verified.

Table 3. Analysis of Variance for full quadratic model.

			(BP) dye		
Source of variation	Df	Sum of square	Mean square	F-value	P-value
Model	14	4253.6	311.90	750..27	< 0.0001
X_1	1	1766.6	1766.6	4229.1	< 0.0002
X_2	1	268.33	268.33	647.91	< 0.0002
X_3	1	140.36	140.36	336.8	< 0.0000
X_4	1	436.95	436.95	1058.1	< 0.0001
X_1X_2	1	386.1	386.1	931.1	< 0.0001
X_1X_3	1	31.35	31.35	74.2	< 0.0000
X_1X_4	1	211.2	211.2	476.4	< 0.0001
X_2X_3	1	13.11	13.11	31.2	< 0.0000
X_2X_4	1	0.485	0.485	1.1911	0.29311
X_3X_4	1	3.1092	3.1092	7.4912	0.0154
X_3X_5	1	226.11	226.11	546.12	< 0.0001
X_1^2	1	33.945	33.945	82023	< 0.0001
X_2^2	1	4.3212	4.3212	10.53	0.00563
X_3^2	1	154.37	154.37	372.63	< 0.0001
X_4^2	15	6.315	0.4217	751.62	< 0.0002
Residual	9	5.1152	0.57632		
Lack of Fit	6	1.0545	0.1763	3.2912	0.080496
Pure Error	29	4361.6			

Response surface methodology (RSM) analysis

Response surface methodology (RSM) was utilized to ameliorate the optimization and estimation of all significance interaction of variables and the relative significance of adsorption processes. Figure 5, exhibits the three-dimensional surface response plots of this interaction. The plots were prepared for a specified pair of factual factors at optimal and fixed values of other variables [32,37]. A positive increase in the (BP) dye removal percentage with the increase in adsorbent mass. Significant diminish in removal percentage of the lower amount of ZIF-67 Modified by Fe_3O_4 NPs is attributed to the higher ratio of (BP) dye molecules to the vacant sites of the adsorbent. Maximum (BP) dye deletion of 100%, the optimum conditions were as follows: pH of 7.0, ultrasound time of 4.0 min, the adsorbent mass of (0.03 g), and initial (BP) dye equal to 10.0 mgL^{-1}, for (BP) dye. Based on the excellent conformity between the experimental and prediction data, successfully for the evaluation and optimization of the influences of the adsorption independent variables on the removal efficiency of (BP) dye from aqueous media with the help of ZIF-67 Modified by Fe_3O_4 NPs [38,39].

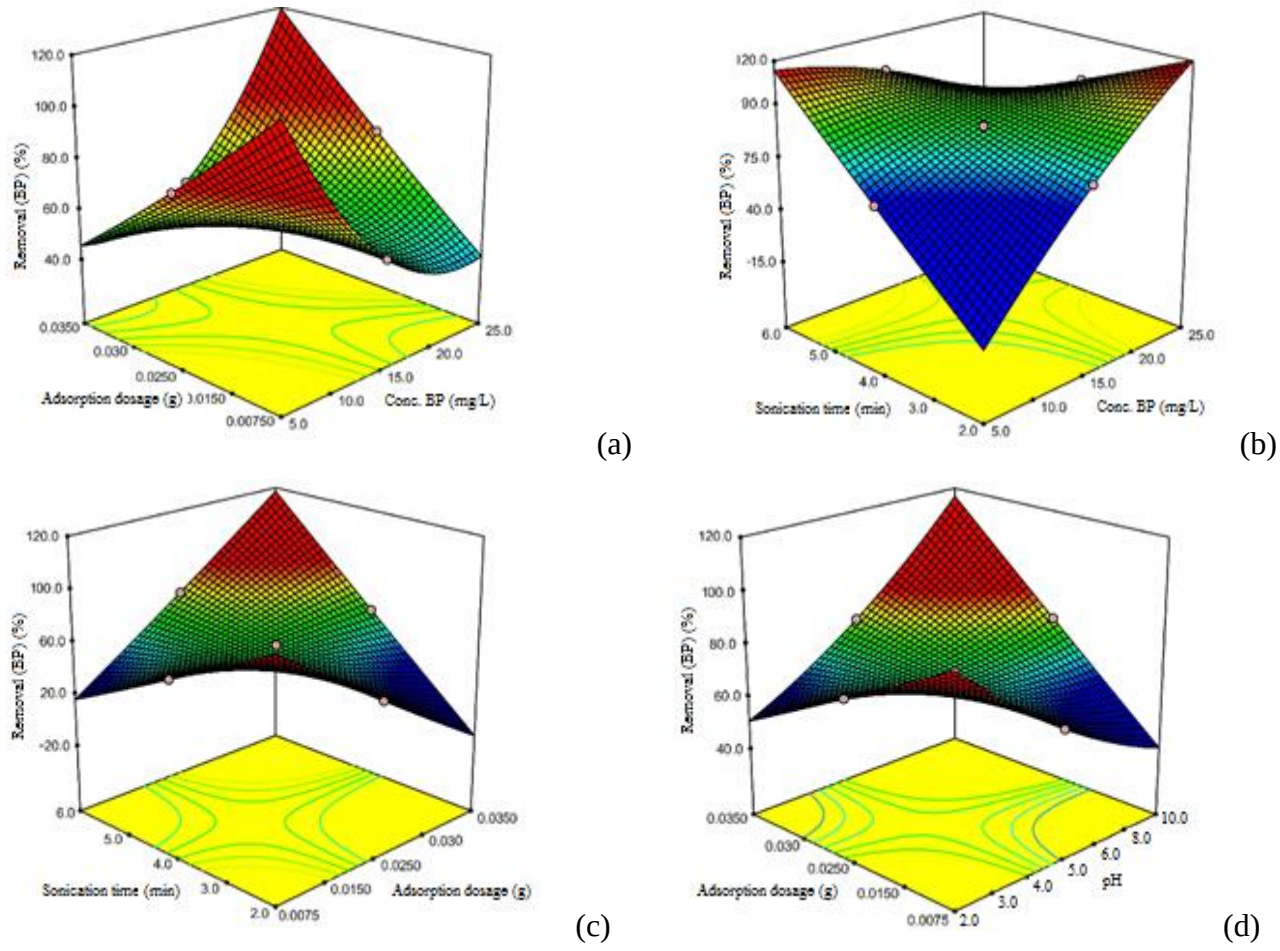

Figure 5. Response surfaces for the dye removal: (a) adsorbent dosage - initial (BP) dye concentration (b) contact time, initial (BP) dye concentration (c) contact time - adsorbent dosage (d) (BP) dye adsorbent dosage (BP) dye – pH.

Restricted to monolayer coverage and the surface was rather uniform the interaction of functional groups with (BP) dye molecule. The highest adsorption capacity for (BP) dye on the ZIF-67 Modified by Fe_3O_4 NPs was estimated to be 92.0 mgg^{-1}.

Optimization of CCD by DF for Extraction Procedure

The profile for desirable option with predicted values in the STATISTICA 10.0 software was used for the optimization of the process (Figure 6). The desirability in the range of 0.0 (undesirable) to 1.0 (very desirable) was used to obtain a global function (*D*) that is the base of optimization. The CCD design matrix results were obtained as maximum (100 %) for (BP) dye respectively. According to these values, DF settings for either of dependent variables of removal percentages were depicted on the side of (Figure 6) [31,38].

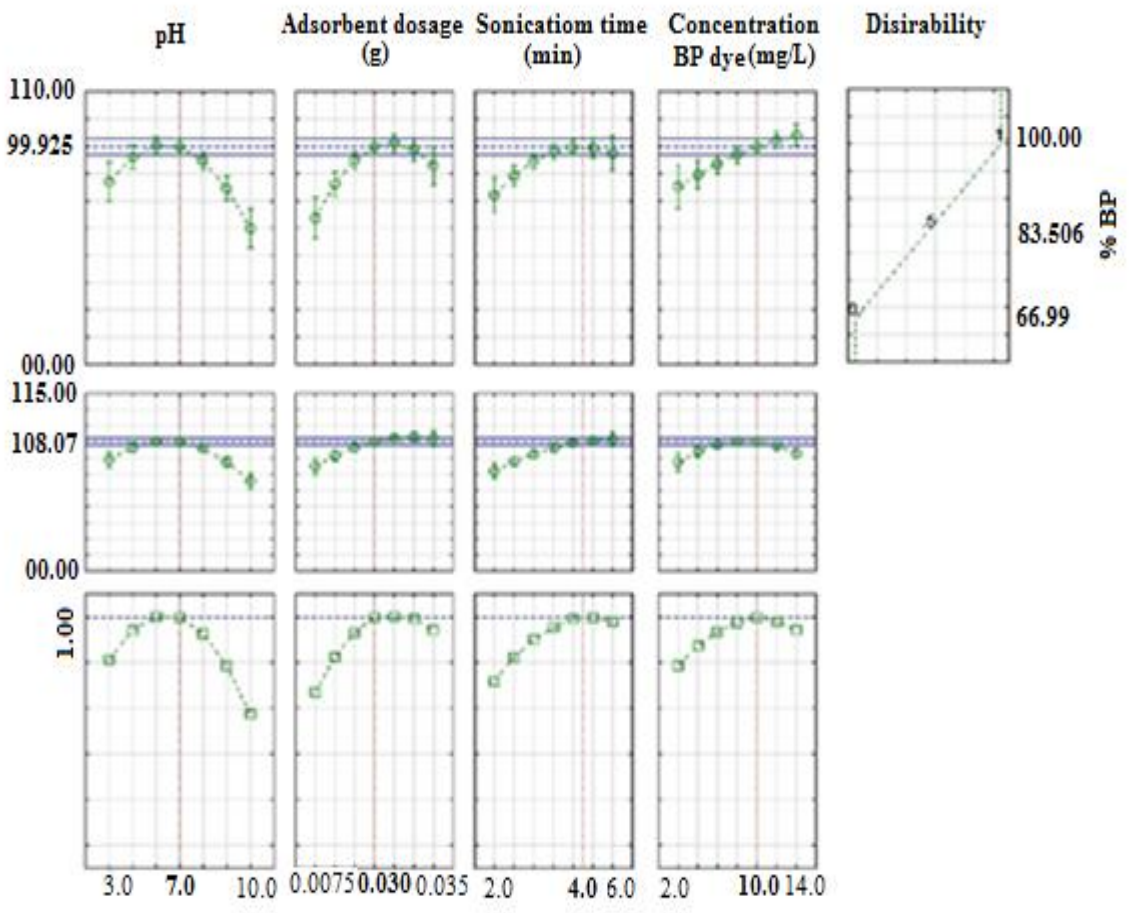

Figure 6. Profiles for predicated values and desirability function for removal percentage of benzyl paraben (BP) dye line indicates current values after optimization.

Adsorption equilibrium study

The experimental adsorption equilibrium data was evaluated for studying the mechanism of (BP) dye adsorption onto ZIF-67 Modified by Fe_3O_4 NPs using different models such as Langmuir, Freundlich, Temkin, and Dubinin-Radushkevich (DR) isotherms [40,41]. In their conventional linear form. Subsequently, their corresponding constants were evaluated from the slopes and intercepts of respective lines (Table 4). These models were applied at optimal dosages of adsorbent while other variables were kept at optimal condition (Table 4). Fitting the experimental data to these isotherm models and considering the higher values of correlation coefficients (R^2 = 0.991) for (BP) dye, that the Langmuir isotherm is the best model to explain the (BP) dye adsorption onto ZIF-67 Modified by Fe_3O_4 NPs, which quantitatively describes the formation of a monolayer of adsorbate on the outer surface of the ZIF-67 Modified by Fe_3O_4 NPs. It also shows the equilibrium distribution of (BP) dye between the solid and liquid phase [42,43].

Table 4. Different isotherm constants and their correlation coefficients calculated for the adsorption of (BP) dye onto ZIF-67 Modified by Fe_3O_4 NPs.

Isotherm	Equation	Parameters	Value of parameters For (BP) dye
Langmuir	$q_e=q_m bC_e/(1+bC_e)$	Q_m (mg g^{-1})	92.0
		K_a (L mg^{-1})	0.465
		R^2	0.997
Freundlich	$\ln q_e = \ln K_F + (1/n) \ln C_e$	1/n	0.53
		K_F (L mg^{-1})	4.12
		R^2	0.962
Tempkin	$q_e = B_1 \ln K_T + B_1 \ln C_e$	B_1	15.2
		K_T (L mg^{-1})	6.795
		R^2	0.932
Dubinin-Radushkevich (DR)	$\ln q_e = \ln Q_s - B\varepsilon^2$	Q_s (mg g^{-1})	38.23
		$B\times 10^{-7}$	-1
		E (kj mol^{-1})	2319
		R^2	0.9423

Kinetic study

In Table 5, the values of the kinetic parameters of pseudo-first-order and second-order [42-44] models as well as qe,cal, qe,exp. and R^2 are represented. As evident, the estimation of the correlation coefficient in the pseudo-second-order equation for the adsorption of (BP) dye onto ZIF-67 Modified by Fe_3O_4 NPs was 0.999. It is worthy of note that the estimated values of qe, cal were

in great conformity with the experimental data. Therefore, it can be assumed that pseudo-second-order rate process can appropriately describe the adsorption of (BP) dye onto ZIF-67 Modified by Fe_3O_4 NPs. The fitness of film diffusion model is indicated by the close to unity value of R^2. However, the fact that the straight lines did not pass through the origin indicate that resistance or film diffusion is not probably the sole rate-limiting step. The calculation of the Elovich constants is possible from the plots of qt versus lnt [44,45]. On the other hand, the inaptness of this model for the adsorption of (BP) dye onto ZIF-67 Modified by Fe_3O_4 NPs adsorbents is apparent from the low values of correlation coefficient (R^2) (Table 5).

Table 5. Kinetic parameters for the adsorption of (BP) dye onto ZIF-67 Modified by Fe_3O_4 NPs.

Model	Parameters	Value of parameters for (BP) dye
Pseudo-first-order kinetic	$k_1(min^{-1})$	0.996
	q_e (calc) (mgg^{-1})	17.12
	R^2	0.9136
Pseudo-second-order kinetic	k_2 (min^{-1})	0.146
	q_e(calc) (mgg^{-1})	55.97
	R^2	0.999
Intraparticle diffusion	K_{diff} (mgg^{-1} $min^{-1/2}$)	8.15
	C (mgg^{-1})	32.98
	R^2	0.9774
Elovich	β (g mg^{-1})	0.917
	α (mgg^{-1} min^{-1})	17.94
	R^2	0.9636

Effect of solution ionic strength

Most dye wastewaters contain salts, and dye adsorption is strongly influenced by the concentration and nature of these ionic species. The presence of any ion could affect. Selected concentrations of NaCl, in the range of (0.01-1.0 M), were added to individual beakers containing 50 ml of the tested (BP) dye solution (10 mg L^{-1}). The solution pH and ZIF-67 and ZIF-67 Modified by Fe_3O_4 NPs dosage were fixed at 7.0 and 0.03 g, respectively, and the stirring time was 4.0 min. The mixing time elapsed, for the residual dyes, results indicated that the adsorption ZIF-67 and ZIF-67 Modified by Fe_3O_4 NPs for (BP) dye were not significantly affected by increasing NaCl concentration. Indicates that Na^+ and Cl^- ions do not compete with the positively or negatively

charged groups of the (BP) dye molecules for being adsorbed onto ZIF-67, and ZIF-67 Modified by Fe_3O_4 NPs. The results seen in (Table 6) [31,45].

Table 6. Effect of the ionic strength on the removal of the (BP) dye onto ZIF-67 Modified by Fe_3O_4 NPs. [C_0 = 10.0 mg L^{-1}, pH = 7.0, dosage sorbent = 0.03 g, time = 4.0 min, T=25^{0}C].

NaCL (M)	R% (BP) dye onto ZIF-67 Modified by Fe_3O_4 NPs	R% (BP) dye onto ZIF-67
0.00	96.7	83.2
0.01	97.0	83.1
0.03	97.4	83.5
0.05	97.0	83.2
0.08	97.5	83.6
0.1	97.6	83.4
0.2	97.5	83.2
0.3	97.8	83.5
0.5	97.6	83.1
0.8	97.2	83.6
1.0	97.1	83.2

Recycling of the adsorbent

The ability to recover, and reusing of the adsorbent was tested in several steps of adsorption, and desorption. The result is shown in (Figure 7). As shown in Figure, 98% of (BP) dye was desorbed from the adsorbent after the first cycle, and after 6 cycles, there were slight changes in (BP) dye desorption. So, it was concluded that the desired removal of 98% could be achieved after 6 cycles [32,43].

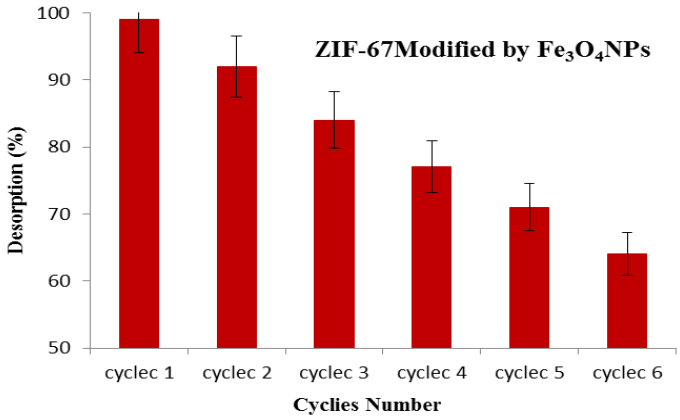

Figure 7: Desorption of (BP) dye from ZIF-67 Modified by Fe_3O_4 NPs. [C_0= 10.0 mgL^{-1}, pH = 7.0, dosage sorbent = 0.03 g, time = 4.0 min, T=25^{0}C].

Comparison of various adsorbent

A comparison of the maximum adsorption capacities of different adsorbents for the removal of (BP) dye was also reported in (Table 7). The outcomes of the table clearly show that the sorption capacity of utilized sorbent in the current study is significantly high. In general, morphology, particle size and distribution and surface structure of this sorbent were effective in its successful outcomes.

Table 7. Comparison of results for this work with other reported.

dye	Adsorbent	Dosage sorbent (g)	Adsorption capacity (mgg^{-1})	References
Benzyl paraben (BP) dye	Mn-doped PbS (PbS:Mn) NPs	0.1	145.0 mgg^{-1}	[3]
Buthyl paraben dye	ALLC AgNPs	0.025	100.0 mgg^{-1}	[6]
Benzyl paraben (BP) dye	Activated carbon (AC)	0.1	11.64 mgg^{-1}	[9]
Benzyl paraben (BP) dye	Il-MNP-ßCD-TDI	0.1	18.48 mgg^{-1}	[25]
Benzyl paraben (BP) dye	ZIF-67 Modified by Fe_3O_4NPs	0.030	92.0 mgg^{-1}	Present study

Conclusion

The applicability of Zeolitic Imidazolate-67 Modified by Fe_3O_4 Nanoparticles, was studied for removal of (BP) dye from wastewater by adsorption method was studied. Response surface methodology was exercised to design the experiments and quadratic model was utilized for the prediction of the variables. The excellent contribution of ZIF-67 Modified by Fe_3O_4 Nanoparticles in deleting (BP) dye was confirmed when the lowest errors were obtained in no time. The use of ZIF-67 Modified by Fe_3O_4 Nanoparticles sorbent as a natural and inexpensive valuable resource and environmentally benign support. According to the results, ZIF-67 Modified by Fe_3O_4 Nanoparticles could as a reusable adsorbent, it would be an economically viable option that can lead to industrial wastewater advancement and high-quality treated effluent.

Abbreviations

BP	Benzyl Paraben
ZIF-67	Zeolitic Imidazolate-67
NPs	Nanoparticles
CCD	Central composite design
RSM	Response surface methodology

C	Initial concentration of dye
Ce	Equilibrium concentration of dye
qe	Amount of dye adsorbed at equilibrium
qt	Amount of dye adsorbed at time
qm	Adsorption capacity
BET	Brunauer–Emmett–Teller
FT-IR	Fourier Transform InfraRed
XRD	X-ray diffraction
SEM	Scanning electron microscopy

Acknowledgement

The authors would like to acknowledge and thank the partial support of the Islamic Azad University, Branch of Ayatollah Amoli, Iran in this work.

References

1. Zarei M, Niaei A, Salari D, Khataee A. Application of response surface methodology for optimization of peroxi-coagulation of textile dye solution using carbon nanotube-PTFE cathode. J Hazard Mater. 2010;173(1–3):544–51.

2. Abbas Ghazali A. Ultrasonic Assisted Removal of Methyl Paraben (MP) on Ultrasonically Synthesized Zn(OH) 2-NPs-AC: Experimental Design Methodology. J Phys Theor Chem IAU Iran). 2021;18(1):65–78.

3. Chemistry T. Adsorption of Benzyl Paraben Dye from Aqueous Solutions Using synthesized Mn- doped PbS (PbS:Mn) nanoparticles Elham Mousavi and Alireza Geramizadegan *. 2021;17:123–43.

4. Karachi N, Motahari S, Nazarian S. Working for the betterment of simultaneous deletion of paraben dyes from industrial effluents on to Origanum majorana-capped silver nanoparticles. Desalin Water Treat. 2021;228:389–402.

5. Maghami F, Abrishamkar M, Goodajdar BM, Hossieni M. Simultaneous adsorption of methylparaben and propylparaben dyes from aqueous solution using synthesized Albizia lebbeck leaves-capped silver nanoparticles. Desalin Water Treat. 2021;228:376–88.

6. Maghami F, Abrishamkar M, Godajdar BM, Hossieni M. Green Fabrication of Albizia Lebbeck Leaves-Capped Silver Nanoparticles for Removal of Butylparaben. Karaj branch J Appl Chem Res. 2022;16:46–64.

7. Mohammadi F, Esrafili A, Sobhi HR, Behbahani M, Kermani M, Asgari E, et al. Evaluation of adsorption and removal of methylparaben from aqueous solutions using amino-functionalized magnetic nanoparticles as an efficient adsorbent: Optimization and modeling by response surface methodology (RSM). Desalin Water Treat. 2018;103:248–60.

8. Pournamdaria E. Response Surface Methodology for Adsorption of Humic Acid by Polyetheretherketone/ Polyvinylalcohol Nanocomposite Modified with Zinc Oxide Nanoparticles from Industrial Wastewater. Pollution. 2023;9(3):965–83.

9. Chen HW, Chiou CS, Wu YP, Chang CH, Lai YH. Magnetic nanoadsorbents derived from magnetite and graphene oxide for simultaneous adsorption of nickel ion, methylparaben, and reactive black 5. Desalin Water Treat. 2021;224:168–77.

10. Azad FN, Ghaedi M, Dashtian K, Hajati S, Pezeshkpour V. Ultrasonically assisted hydrothermal synthesis of activated carbon-HKUST-1-MOF hybrid for efficient simultaneous ultrasound-assisted removal of ternary organic dyes and antibacterial investigation: Taguchi optimization. Ultrason Sonochem. 2016;31:383–93.

11. Malek NNA, Jawad AH, Abdulhameed AS, Ismail K, Hameed BH. New magnetic Schiff's base-chitosan-glyoxal/fly ash/Fe3O4 biocomposite for the removal of anionic azo dye: An optimized process. Int J Biol Macromol. 2020;146:530–9.

12. Reghioua A, Barkat D, Jawad AH, Abdulhameed AS, Al-Kahtani AA, Alothman ZA. Parametric optimization by Box-Behnken design for synthesis of magnetic chitosan-benzil/ZnO/Fe3O4nanocomposite and textile dye removal. J Environ Chem Eng. 2021;9(3):105166.

13. Ganiyu SA, Suleiman MA, Al-Amrani WA, Usman AK, Onaizi SA. Adsorptive removal of organic pollutants from contaminated waters using zeolitic imidazolate framework Composites: A comprehensive and Up-to-date review. Sep Purif Technol. 2023;318(January).

14. Bhattacharjee S, Jang MS, Kwon HJ, Ahn WS. Zeolitic Imidazolate Frameworks: Synthesis, Functionalization, and Catalytic/Adsorption Applications. Catal Surv from Asia. 2014;18(4):101–27.

15. Marahel F, Mombeni Goodajdar B, Niknam L, Faridnia M, Pournamdari E, Mohammad Doost S. Ultrasonic assisted adsorption of methylene blue dye and neural network model for adsorption of methylene blue dye by synthesised Mn-doped PbS nanoparticles. Int J Environ Anal Chem. 2023;103(13):3059–80.

16. Zhang J, Yang X, Cheng S, Zou D, Cheng F. Preparation of core-shell TiO2@ZIF-67 and its effective adsorption of methyl orange from water. Desalin Water Treat. 2022;261:266–77.

17. Al-Hazmi GH, Adam AMA, El-Desouky MG, ElBindary AA, Alsuhaibani AM, Refat MS. EFFICIENT ADSORPTION OF RHODAMINE B USING A COMPOSITE OF Fe3O4@ZIF-8: SYNTHESIS, CHARACTERIZATION, MODELING ANALYSIS, STATISTICAL PHYSICS AND MECHANISM OF INTERACTION. Bull Chem Soc Ethiop. 2023;37(1):211–29.

18. Chen L, Zhang X, Cheng X, Xie Z, Kuang Q, Zheng L. The function of metal-organic frameworks in the application of MOF-based composites. Nanoscale Adv. 2020;2(7):2628–47.

19. Arabkhani P, Javadian H, Asfaram A, Ateia M. Decorating graphene oxide with zeolitic imidazolate framework (ZIF-8) and pseudo-boehmite offers ultra-high adsorption capacity of diclofenac in hospital effluents. Chemosphere. 2021;271:129610.

20. Hajializadeh A, Ansari M, Foroughi MM, Jahani S, Kazemipour M. Zeolite Imidazolate

Framework Nanocrystals Electrodeposited on Stainless Steel Fiber for Determination of Polycyclic Aromatic Hydrocarbons. Iran J Chem Chem Eng. 2022;41(2):368–79.

21. Si Y, Wang W, El-Sayed ESM, Yuan D. Use of breakthrough experiment to evaluate the performance of hydrogen isotope separation for metal-organic frameworks M-MOF-74 (M=Co, Ni, Mg, Zn). Sci China Chem. 2020;63(7):881–9.

22. Feng Z, Zhu J, Zhuo S, Chen J, Huang W, Cheng H, et al. Magnetic/Zeolitic Imidazolate Framework-67 Nanocomposite for Magnetic Solid-Phase Extraction of Five Flavonoid Components from Chinese Herb Dicranopteris pedata. Molecules. 2023;28(2).

23. Pooladi H, Foroutan R, Esmaeili H. Synthesis of wheat bran sawdust/Fe3O4 composite for the removal of methylene blue and methyl violet. Environ Monit Assess. 2021;193(5).

24. Zubair M, Jarrah N, Ihsanullah, Khalid A, Manzar MS, Kazeem TS, et al. Starch-NiFe-layered double hydroxide composites: Efficient removal of methyl orange from aqueous phase. J Mol Liq. 2018;249:254–64.

25. Md Yusoff M, Yahaya N, Md Saleh N, Raoov M. A study on the removal of propyl, butyl, and benzyl parabens: Via newly synthesised ionic liquid loaded magnetically confined polymeric mesoporous adsorbent. RSC Adv. 2018;8(45):25617–35.

26. Foroutan R, Peighambardoust SJ, Hemmati S, Khatooni H, Ramavandi B. Preparation of clinoptilolite/starch/CoFe2O4 magnetic nanocomposite powder and its elimination properties for cationic dyes from water and wastewater. Int J Biol Macromol. 2021;189(June):432–42.

27. Wu Z, Wang Y, Xiong Z, Ao Z, Pu S, Yao G, et al. Core-shell magnetic Fe3O4@Zn/Co-ZIFs to activate peroxymonosulfate for highly efficient degradation of carbamazepine. Appl Catal B Environ. 2020;277(May):119136.

28. Rubab M, Bhatti IA, Nadeem N, Shah SAR, Yaseen M, Naz MY, et al. Synthesis and photocatalytic degradation of rhodamine B using ternary zeolite/WO 3 /Fe 3 O 4 composite. Nanotechnology. 2021 Aug 20;32(34):345705.

29. Mphuthi LE, Erasmus E, Langner EHG. Metal Exchange of ZIF-8 and ZIF-67 Nanoparticles with Fe(II) for Enhanced Photocatalytic Performance. ACS Omega. 2021;6(47):31632–45.

30. Fernandes E, Contreras S, Medina F, Martins RC, Gomes J. N-doped titanium dioxide for mixture of parabens degradation based on ozone action and toxicity evaluation: Precursor of nitrogen and titanium effect. Process Saf Environ Prot. 2020;138:80–9.

31. Einolghozati S, Pournamdari E, Choobkar N, Marahel F. Response surface methodology for removal of methyl violet dye using Albizia stem bark Lebbeck modified by Fe2 (MoO4)3 nanocomposite from aqueous solutions and assessment relative error by neural network model. Desalin Water Treat. 2022;278:195–208.

32. Yu F, Bai X, Liang M, Ma J. Recent progress on metal-organic framework-derived porous carbon and its composite for pollutant adsorption from liquid phase. Chem Eng J. 2021;405(September 2020):126960.

33. Kiani M, Bagheri S, Karachi N, Alipanahpour Dil E. Adsorption of purpurin dye from industrial wastewater using Mn-doped Fe2O4 nanoparticles loaded on activated carbon. Desalin Water Treat. 2019;152(August):366–73.

34. Khan A, Ali M, Ilyas A, Naik P, Vankelecom IFJ, Gilani MA, et al. ZIF-67 filled PDMS

mixed matrix membranes for recovery of ethanol via pervaporation. Sep Purif Technol. 2018;206(April):50–8.

35. Li Y, Jin Z, Zhao T. Performance of ZIF-67 – Derived fold polyhedrons for enhanced photocatalytic hydrogen evolution. Chem Eng J. 2020;382(October 2019):123051.

36. Habbal S, Haddou B, Canselier JP, Gourdon C. Easy removal of methylparaben and propylparaben from aqueous solution using nonionic micellar system. Tenside, Surfactants, Deterg. 2019;56(2):112–8.

37. Bagheri S, Aghaei H, Ghaedi M, Asfaram A, Monajemi M, Bazrafshan AA. Synthesis of nanocomposites of iron oxide/gold (Fe3O4/Au) loaded on activated carbon and their application in water treatment by using sonochemistry: Optimization study. Ultrason Sonochem. 2018;41:279–87.

38. Pargari M, Marahel F, Godajdar BM. Ultrasonic-assisted adsorption of propyl paraben on ultrasonically synthesized TiO2 nanoparticles loaded on activated carbon: Optimization, kinetic and equilibrium studies. Desalin Water Treat. 2021;212:164–72.

39. Nasab SG, Semnani A, Teimouri A, Yazd MJ, Isfahani TM, Habibollahi S. Decolorization of crystal violet from aqueous solutions by a novel adsorbent chitosan/nanodiopside using response surface methodology and artificial neural network-genetic algorithm. Int J Biol Macromol. 2019;124:429–43.

40. Hajati S, Ghaedi M, Barazesh B, Karimi F, Sahraei R, Daneshfar A, et al. Application of high order derivative spectrophotometry to resolve the spectra overlap between BG and MB for the simultaneous determination of them: Ruthenium nanoparticle loaded activated carbon as adsorbent. J Ind Eng Chem. 2014;20(4):2421–7.

41. Marahel F, Mombeeni Goodajdar B, Basari N, Niknam L, Ghazali AA. Applying Neural Network Model for Adsorption Methyl Paraben (MP) Dye Using Ricinus Communis-capeed Fe3O4 NPs Synthesized from Aqueous Solution. Iran J Chem Chem Eng. 2022;41(7):2358–77.

42. Marahel F. Adsorption of hazardous methylene green dye from aqueous solution onto tin sulfide nanoparticles loaded activated carbon: Isotherm and kinetics study. Iran J Chem Chem Eng. 2019;38(5):129–42.

43. Bouroumand S, Marahel F, Khazali F. Removal of yellow he4g dye from aqueous solutions using synthesized mn-doped pbs (Pbs:Mn) nanoparticles. Desalin Water Treat. 2021;223:380–92.

44. Davoudi S. Adsorption of Methylene Blue (MB) Dye Using NiO-SiO2NPs Synthesized from Aqueous Solutions: Optimization, Kinetic and Equilibrium Studies. Iran J Chem Chem Eng. 2022;41(7):2343–57.

45. Ghazimokri HS, Aghaie H, Monajjemi M, Gholami MR. Removal of Methylene Blue Dye from Aqueous Solutions Using Carboxymethyl-β-Cyclodextrin-Fe3O4 Nanocomposite: Thermodynamics and Kinetics of Adsorption Process. Russ J Phys Chem A. 2022 Feb 6;96(2):371–80.